A Novel Approach for Actin Bundle Identification and Analysis in Fluorescence Microscopy Images

Malek L Hamed, Tian Lan, and Yiider Tseng

College of Engineering, University of Florida

Analysis of filamentous actin structures in microscope images is a frequent step in cell research. This analysis is commonly qualitative and based on human inspection, limiting accuracy and quantitative import. Current alternatives involve specialized equipment, require high-resolution images, or limit the structural information that can be extracted. Here, a new approach is developed and applied to wide-field fluorescence microscopy images of actin-stained cells. This analysis was successfully used to extract data regarding individual filament bundles and produce distributional information. A few weaknesses are noted, including occasional erroneous segmentation of intersecting filament bundles and poor results for high-noise images. Future work should investigate the relationships between extracted structural information and physical parameters of filament bundles to strengthen and broaden inference potential.

INTRODUCTION

Effective analysis of the filamentous actin cytoskeleton is key to many areas of cell research. Investigation into the relationship between the structure of the actin cytoskeleton and other variables, such as cell cycle progression [1], action of signaling molecules [2], and extracellular attachment [3], is an active area of research. Analysis required in this research frequently consists of qualitative inspection of fluorescence microscopy images by a human investigator [4], presenting problems of consistency, accuracy, and time. This also limits the quantitative data that can be gathered from samples, restricting its import.

Actin filaments exist as double helix structures with diameters of approximately 7 nm [5]. While these are too small to be observed individually using typical fluorescence microscopy, higher-order bundles can be observed and are the focus of this work. The stress fiber, an actin bundle structure of particular interest here, exists on the order of tenths of a micrometer in diameter [6]; other types of actin bundles have similar diameters [7].

Current approaches for producing quantitative information about subcellular fibrillar structures include pre- and post-imaging methods [4]. Pre-imaging methods use specialized equipment to directly produce data regarding organization and structure. These approaches include the use of polarization microscopy used, for example, to gain data regarding yeast septin filaments [8], and x-ray scattering, as used by Müller and coworkers to study microfibril arrangements within cellulose fibers [9]. These methods, however, require resources not readily available to most labs and are not as easily melded with the techniques familiar to cell biology researchers.

Post-imaging methods involve computational processing of microscope images to identify regions corresponding to fibrillar structures of interest and subsequent analysis. Researchers have used methods based on skeletonization by morphological thinning, as in [10] and [11], and intensity thresholding, as used in the University of North Carolina's Network Extractor (http://cismm.web.unc.edu/software/). These and alternatives [12] tend to be designed for high-resolution images such as those captured by scanning electron microscopy and electron tomography, where individual fibers are distinct. While they provide detailed information about network structure, they generally are not designed to describe structural parameters such as fiber diameter and length.

Newer software tools have attempted to correct some of the problems of accuracy and usability associated with existing approaches. FibrilTool is an ImageJ plug-in that works with readily-producible fluorescence microscope images to provide orientation and anisotropy information [4]. It is, however, not designed to describe individual fiber bundles. SOAX is another tool for studying fibrillar networks [13]. This tool infers thicknesses from pixel intensities along filament centerline, rather than maintaining the original filament signals in entirety. An alternative approach is here attempted.

In this study, I aim to design a computerized analysis tool able to identify filamentous actin bundles in cell fluorescence microscopy images and therewith extract structural and organizational information including bundle diameter, length, and orientation, with minimal human input. It is hypothesized that, by appropriately subsampling cell images and extracting orientation information, I will be able to construct segmentation masks for individual fiber bundles and produce useful data.

MATERIALS AND METHODS

Code was developed in Matlab and utilizes functions provided in its Image Processing Toolbox (http://www.mathworks.com/).

I will hereafter favor the term "filaments" in place of "actin filament bundles" for conciseness and in reflection

of the proposed potential to extend this technique to other filament types.

The filament identification algorithm consists of

1. Image subsampling
2. Identification of subsample principle orientations and filament subdivisions
3. Filament reconstruction based on parameter matching between subdivisions

This algorithm functions on the following premises:

1. By subsampling an image into appropriately-sized bins, filaments can be divided into essentially straight subdivisions with identifiable principle axis orientations.
2. Using this directionality information, we can identify oriented filament subdivisions otherwise indistinguishable with standard thresholding techniques.

The user sets the sampling bin size to begin analysis, considering the pixel width-to-distance scaling factor. A bin size of approximately 1 µm × 1 µm seems optimum for the sizes of actin bundles commonly observed.

The software first subsamples a provided grayscale image into S/n^2 subsamples, where S is the area in square pixels of the image and n is the bin width in pixels. By intensity thresholding, the program selects subsamples located within the cell. Within each subsample, the principle orientation (i.e. the orientation of the subdivided filament contained within the subsample) is determined considering (1) the *ratio of variations* (ROV) and (2) peak prominences. ROV (Figure 1) is a novel parameter that I present for determining orientations of filamentous signals. ROV is based on the assumption that the signal intensity of a sample containing an oriented filamentous signal will show minimum variation when the sample is traversed along the direction of the filament and maximum variation when traversed perpendicularly.

Another parameter used in calculating ROV is the *mean directional profile* (MDP). I define the MDP of a subsample at an angle α as the array of mean intensities of pixel cross-sections (green segments in Figure 1) arranged perpendicularly to α. That is, the mean intensity of the pixels along each green line segment is calculated and arranged consecutively.

To calculate the ROV of a subsample from the MDP, (1) the MDP at each 10-degree interval in a 180-degree range of orientations is calculated. Then, (2) the MDP's range (*r*, i.e. maximum – minimum) is calculated at each angle to determine the variation of intensity values along α. Finally, (3) the ROV at each angle is determined by finding the ratio of the range, r_0, at that angle to that calculated for the angle oriented perpendicularly to it, r_{90}.

$$ROV(\alpha) = \frac{r_0}{r_{90}} = \frac{\max(MDP_0) - \min(MDP_0)}{\max(MDP_{90}) - \min(MDP_{90})}$$

Equation 1. Calculation of ROV at an angle α.

The algorithm also calculates the prominences of peaks within the MDP at each angle, based on the assumption that more prominent peaks will be observable when the sample is traversed perpendicular to the direction of its filament(s). ROVs and peak prominences calculated for a representative subsample are shown in Figure 2. Finally, the principle orientation of the filament subdivision within a subsample is determined by locating the maximum of the element-wise multiplication of the ROV and peak prominence profiles and adding 90° (Figure 2C).

The result of this process is an *orientation matrix*, which contains the principle orientation of each relevant subsample of the original image.

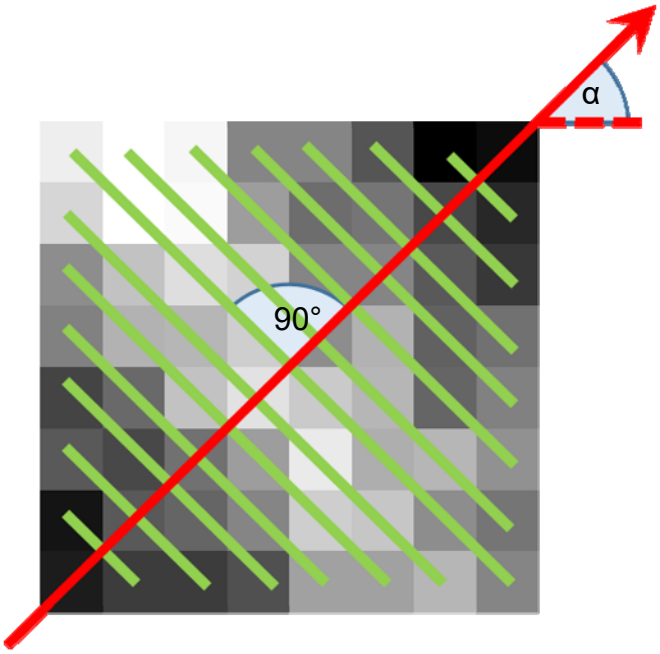

Figure 1. The MDP at α is calculated by taking pixel cross-sections (green lines) directed at α + 90° and calculating the mean intensities of pixels along each. For consistency and to reduce the influence of noise, all cross-sections are set to be equal in length to the longest, central cross-section (in this case, along the square's diagonal), such that non-central cross-sections extend beyond the subsample. This yields an MDP corresponding to the angle α, which is a profile of these mean values. To determine ROV, the MDP is calculated at each 10 degree interval along a 180 degree array of α values, and the range for each MDP is calculated. Then, the ratio of the MDP range at each α to that at α + 90° is calculated, resulting in the ROV profile for the subsample.

Identification of Filament Subdivisions

The software then identifies oriented filament subdivisions within each subsample. I assume that a bundle's diameter is related to the full width at half maximum (FWHM) of its associated linear signal, although I have not found studies clearly explaining this assumption.

Pending further research, for the purposes of this analysis, I assume that the FWHM of the MDP is equivalent to four times the fiber diameter.

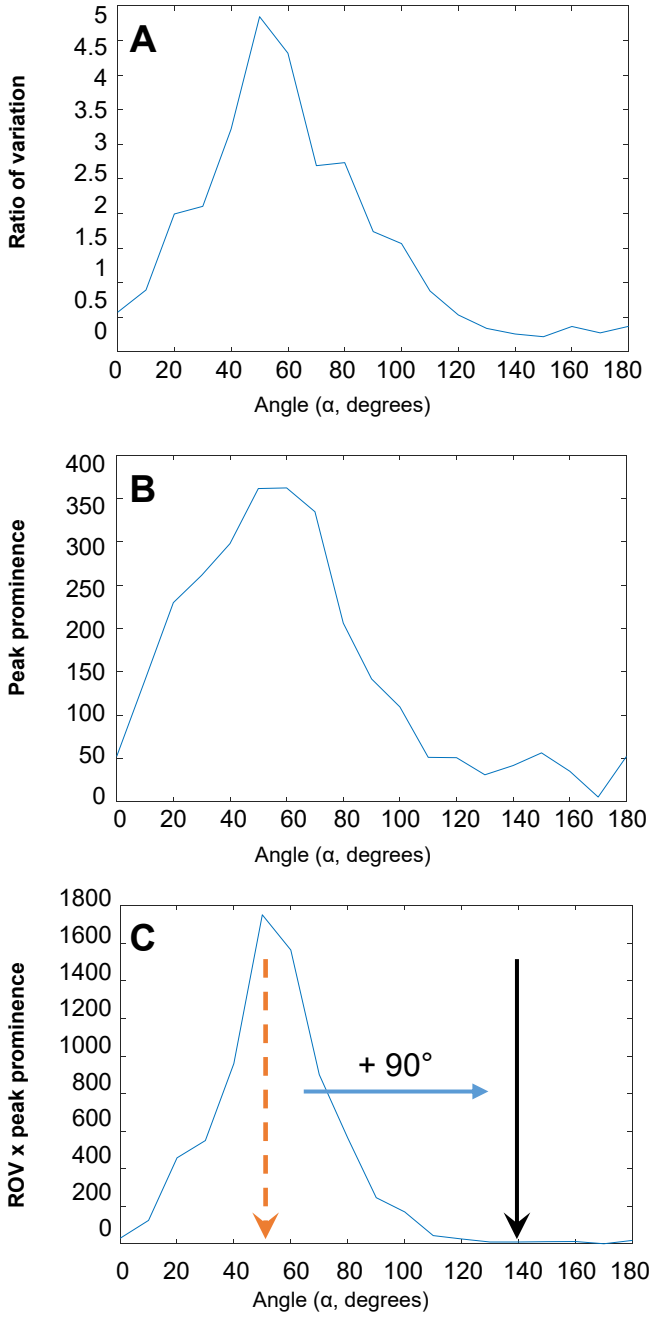

Figure 2. After calculating the ROV profile (A) and peak prominence profile (B) for a given subsample, these are multiplied element-by-element (C), the angle corresponding to the maximum of the resulting array (red dashed arrow) is located, and the principle orientation is identified at 90° greater (black arrow).

Therefore, for each subsample, the program calculates the maximum and FWHM of the MDP perpendicular to the principle orientation. A value of 'true' is then assigned to a corresponding linear segment in the processed image. Linear segments of adjacent subsamples in contact with one another and with a difference in principle orientation less than a threshold value are identified as belonging to the same original filament bundle; these are given a common integer identifier to distinguish them. The result is a matrix of integer identifiers specifying grouped subdivisions of the original filament bundles. Due to image aberrations and other imperfections, this step does not produce entirely unbroken regions associated with contiguous filament bundles.

Rejoining of Detached Segment Groups

The final step in the identification of individual filament bundles is to rejoin detached segment groups that should be contiguous.

First, an orientation is assigned to each sement group by producing an ellipse with the same second moments as the region of grouped segments and then determining the angle of its major axis with respect to the positive x axis. This is achieved using an inbuilt function of Matlab's Image Processing Toolbox.

Next, the program identifies grouped segment regions that (1) are adjacent (i.e. with associated pixels in direct contact) and (2) have orientations differing by less than a threshold. These are then assigned a common integer identifier to categorize them as a unique filament bundle. This image is processed to remove sufficiently small or abnormally shaped regions.

Filament Bundle Analysis

The program analyzes each unique filament within the processed image using Matlab's Image Processing toolbox, yielding the following parameters:

1. *Orientation*. Determined by calculating an ellipse with the same second moments as the filament and determining the angle that its major axis makes with the positive x axis.
2. *Length*. A rough estimate is obtained by calculating the length of the corresponding ellipse's major axis.
3. *Diameter*. Assuming that filament diameter is proportional to FWHM of the raw signal, we can estimate the diameter by dividing the area of the connected component by its length.

From this primary information, we can then calculate additional higher-order information about the filamentous cytoskeleton. Orientation distributions, a diameter distribution, and a diameter-versus-orientation distribution were produced.

Cell Preparation and Microscopy

This system was applied to two cell images for assessment. The cells were NIH 3T3 fibroblasts fluorescently stained for actin. Fixation buffer consisted of

4% paraformaldehyde and 0.5% Triton X-100 in phosphate buffered saline (PBS), and blocking buffer consisted of 2% bovine serum albumin and 0.02% Triton X-100 in PBS. Fixation buffer and blocking buffer were applied consecutively to the cells on coverslips for 30 minutes each at room temperature. Cells were then stained with a 1:40 dilution of Alexa Fluor 568-phalloidin (Sigma-Aldrich) in the secondary antibody solution.

Cells were visualized using a TE-2000 imaging acquisition system with a 60× objective, a Cascade:1K CCD camera, and an X-cite 120 PC fluorescent light source. Acquisitions were conducted with a 500-ms exposure time, no binning, and 100% light intensity.

RESULTS

Filament Identification

The tool was first tested upon the artificial image in Figure 3A, which represents well-defined, high-contrast filaments against a dark background. The results after filament identification and regoining are shown in Figures 3B and 3C, respectively

The four short parallel lines at the upper left of the image were segmented as distinct, intact filaments. The three segments to the right were each segmented into two portions. Inappropriate divisions were identified at intersections between 'fibers.' The software was able to identify regions before and after the sharp curve at the far right as belonging to a single fiber.

The identification program was then applied to a cell image with clearly defined bundles. Individual bundles were generally recognized correctly. As apparent in Figure 4, the closely spaced parallel bundles at the center of the cell were identified as distinct. Occasional error in distinguishing adjacent, parallel bundles is apparent as demonstrated in Figure 4C. Contiguous fibers also generally remained intact after the final step, although occasional errors are evident.

We finally tested the filament identification method on a high-noise image with less clearly-defined actin bundles (Figure 5A). While the fibers of high intensity in the center of the cell were segmented mostly as distinct and intact, the fibers in the less intense regions of the cell area were not consistently identified; irrelevant segmentations were generated in these regions (Figure 5C).

Distributional and holistic analysis

From the raw image in Figure 4A, we produced: (1) an orientation distribution, (2) a length-weighted orientation distribution, (3) a diameter distribution, (4) a distribution of filament diameters with respect to orientation.

Orientation distribution. This distribution is shown in Figure 7A. It agrees with a visual inspection of the raw image, which suggests a preponderance of filaments oriented approximately -60° and 40° relative to the positive x axis.

Length-weighted orientation distribution. Figure 7B shows the orientation data with frequency weighted with respect to filament length at the given orientation. This emphasizes the -60° and 40° peaks observed previously in the raw cell image. This method of weighting can similarly be applied with respect to other parameters produced by the analysis program.

Diameter distribution. As shown in Figure 7C, we observe a skewed distribution with a majority of low-diameter filaments.

Diameter distribution relative to orientation. This distribution (Figure 7D) was produced to assess the potential for comparing relationships between multiple parameters of filament structure. Maximum diameters occur at orientations of approximately -60° and 50° relative to the positive x axis, which agrees with a visual inspection of the raw image.

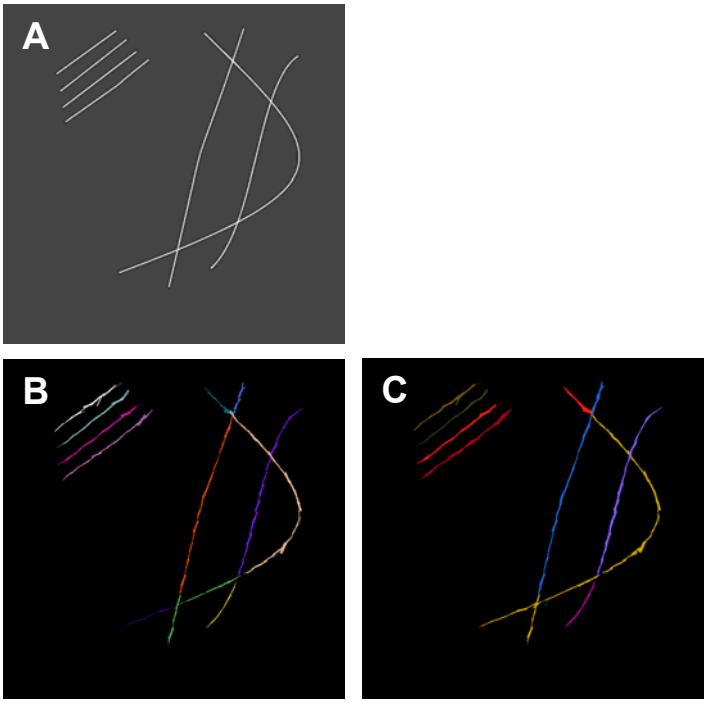

Figure 3. Segmentation of a mock filament image. (A) shows the original. (B) is the image after the initial identification process. Unique colors indicate distinct identified filaments. The three linear segments at the top left are correctly identified as distinct and intact, while the overlapping segments to the right are each segmented into multiple fragments. (C) is the result after the rejoining process. Segmentation is correct except for three incorrect divisions occurring at intersections of the filaments at the right.

DISCUSSION

Analysis of filamentous structures in microscope images of cells is an important step in many areas of research. A novel method for identifying and analyzing filamentous actin bundles in fluorescent microscope images of cells

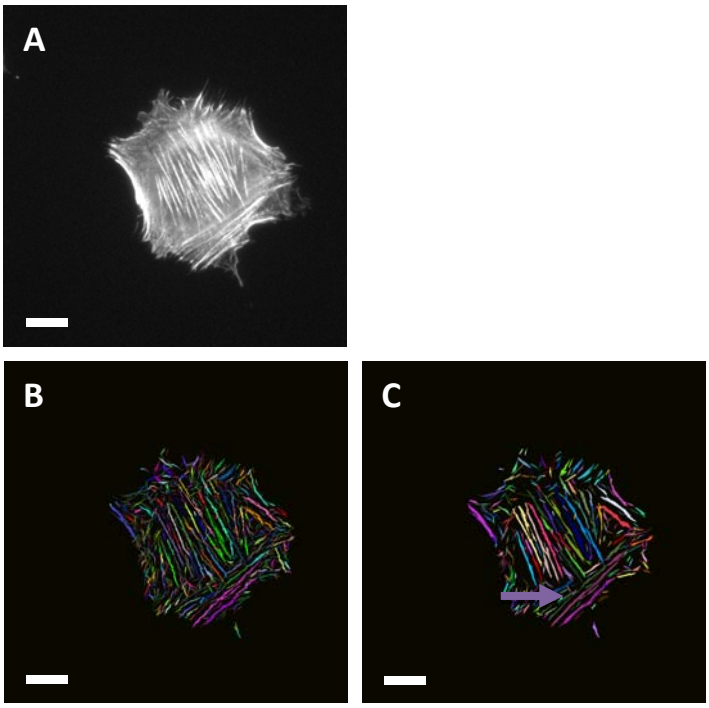

Figure 4. Segmentation of a clear cell image. (A) shows the original. (B) is the image after the initial identification process. Unique colors indicate distinct identified filaments. After this step, incorrect intra-filament divisions remain. (C) Noise segments have been removed, and most intra-filament divisions have been corrected. Occasional joining of distinct filaments is noted (yellow arrow). Scale bar = 50 μm.

was here developed and applied to two distinct cell images, with success when in the low-noise case.

The system allows for description of individual actin filament bundles within a segmented image, making it, to my knowledge, unique in this regard. More evidently useful is its ability to extract distributional information; potentially allowing for the study of cytoskeletal structure under different conditions and for investigation of the relationships between various parameters of filament organization. Whereas these types of analyses are commonly performed visually or using ad hoc analysis tools, this system can potentially allow for large-scale automated analyses, yielding quantitative data for statistical analysis.

Segmentation is not error-free. Parallel bundles in close adjacency are occasionally identified as contiguous, and fibers are occasionally disjoined, especially at regions of intersection. While this segmentation algorithm makes it difficult to guarantee avoiding these errors, it is expected that postprocessing can help to rectify these faults.

Generation of distribution data demonstrates a robust feature. Weighted and unweighted orientation distributions illustrate the potential for researchers to produce information in accordance with their particular research needs, such as filament orientations assessed relative to their lengths, allowing for the investigation of filament anisotropy. Additionally, the construction of a diameter vs. orientation distribution illustrates how assumptions may be used to draw conclusions. For example, a clarification of the relationship between filament diameter and tensile strength may allow investigators to study the mechanical state of cells along various orientations.

It is notable that analysis of bundle diameters yielded a skewed distribution. This may be the result of the identification of false small filaments. Further investigation is required.

This program holds a few notable weaknesses. Firstly, processing is lengthy, requiring one to two minutes per image, but since it is automated, this may not be a practical problem. Secondly, it cannot distinguish overlapping, parallel fibers as may occur in wide-field microscopy; therefore, the program may be more effectively applied to confocal images. Such images carry less interference from out-of-focus structures, potentially making them particularly amenable to this approach.

Future work should investigate the relationships between the parameters outputted by this system and physical properties of cells, such as the association between FWHM and filament diameter. Bundle diameters calculated in this study, while on the same order magnitude of those reported

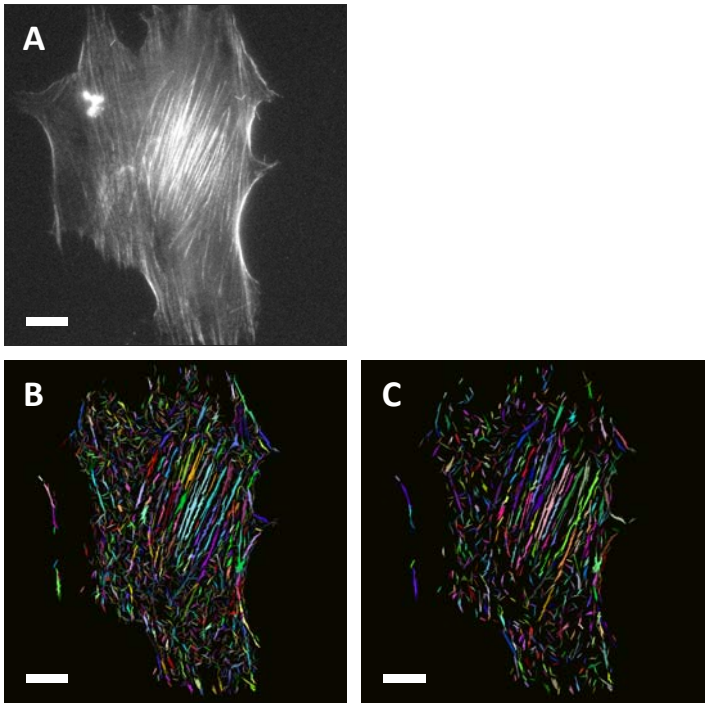

Figure 5. Segmentation of a high-noise image. (A) shows the original. (B) is the image after the initial identification process. Unique colors indicate distinct identified filaments. After this step, incorrect intra-filament divisions remain, as well as a large degree of irrelevant segmentation in areas corresponding to low contrast in the original image. (C) While most intra-filament divisions are corrected after this step, much noise remains, and most filaments in the low contrast regions remain unsegmented. Scale bar = 50 μm.

in the literature, were larger by roughly a factor of three on average. Use of an unverified inference of bundle diameter (i.e. one-fourth signal FWHM) as a placeholder for a more conclusive relationship likely contributed. The discrepancy

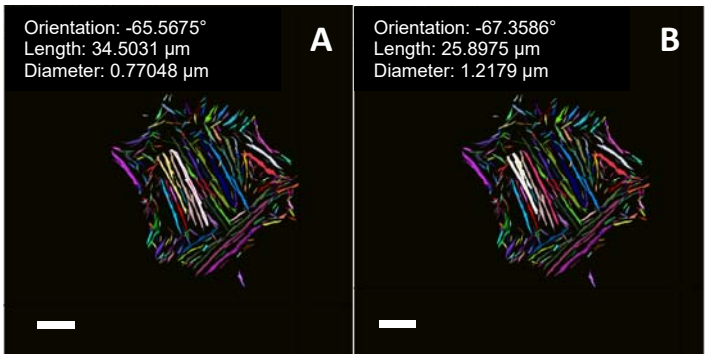

Figure 6. (A) Analysis of the filament outlined in white yields the estimated parameters shown, which are in approximate agreement with a visual inspection of the raw image. (B) shows the analysis applied where branching is identified, leading to overestimation of bundle diameter. Scale bar = 50 µm.

is therefore reasonable. More robust methods for analyzing filament segmentations might be developed to allow for more accurate estimations of parameters such as diameter and to describe additional features such as curvature.
more accurate estimations of parameters such as diameter, and to describe additional features such as curvature.

ACKNOWLEDGEMENTS

Sincere thanks go to Probal Guha for his valuable guidance.

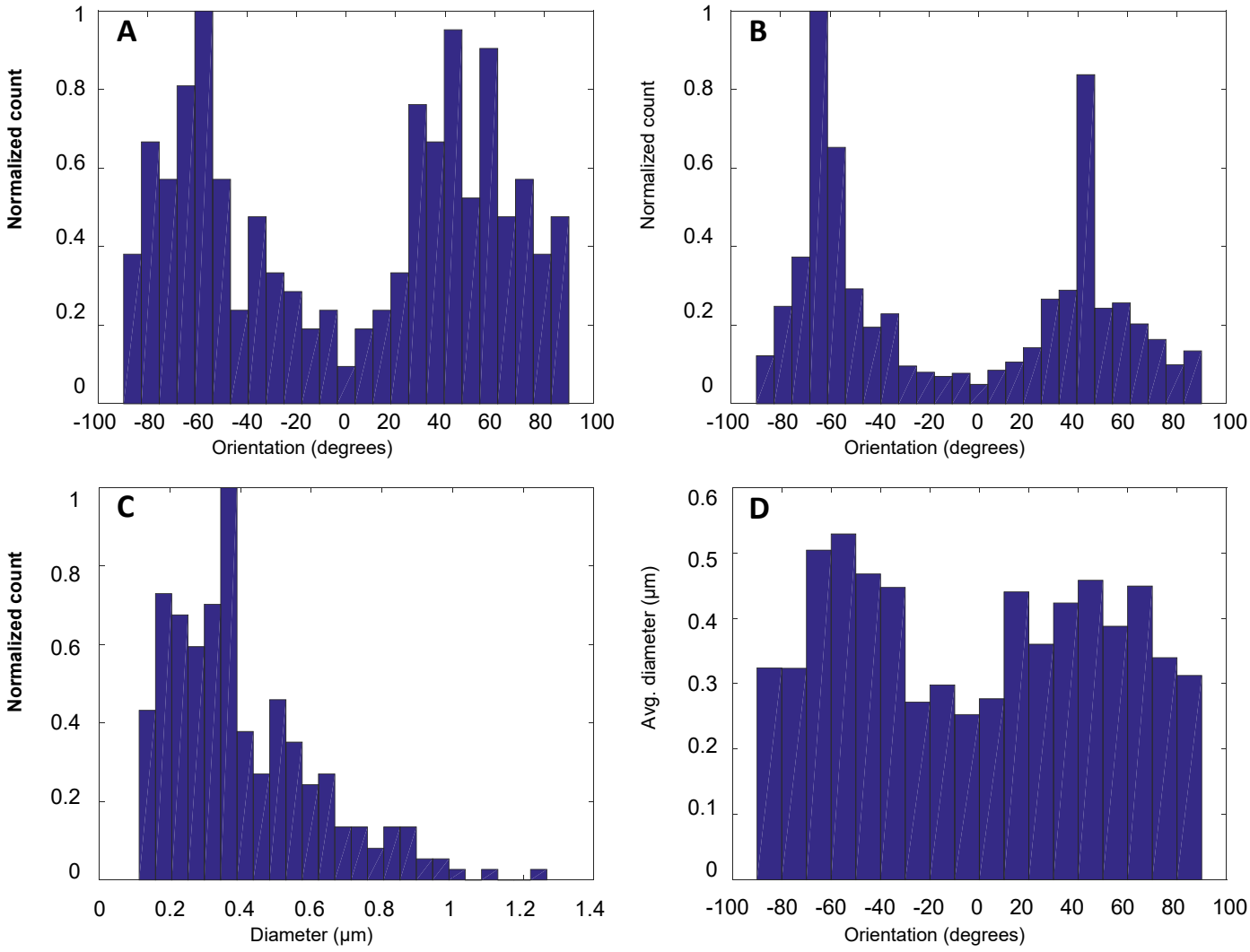

Figure 7. (A) shows an orientation distribution, showing the relative number of detected filament bundles at orientations relative to the positive x axis. Peaks are clearly apparent around -60° and 40°, which appears to agree with the raw image. (B) shows a length-weighted orientation distribution, such that the frequency of filaments at a given orientation is weighted with respect to the lengths of the corresponding filaments. The peaks previously observed at -60° and 40° are thus emphasized. (C) shows a diameter distribution, skewed with a majority of low diameter filaments. (D) shows a comparative distribution of average diameter relative to filament orientation. Maximum filament diameters are suggested to exist at approximately -60° and 50° relative to the positive x axis, apparently in agreement with the raw image.

REFERENCES

[1] T. Yamagishi and H. Kawai, "Cytoskeleton Organization during the Cell Cycle in Two Stramenopile Microalgae, Ochromonas danica (Chrysophyceae) and Heterosigma akashiwo (Raphidophyceae), with Special Reference to F-actin Organization and its Role in Cytokinesis", Protist, vol. 163, no. 5, pp. 686-700, 2012.

[2] S. Mana-Capelli, M. Paramasivam, S. Dutta and D. McCollum, "Angiomotins link F-actin architecture to Hippo pathway signaling", Molecular Biology of the Cell, vol. 25, no. 10, pp. 1676-1685, 2014.

[3] D. Hanein and A. Horwitz, "The structure of cell–matrix adhesions: the new frontier", Current Opinion in Cell Biology, vol. 24, no. 1, pp. 134-140, 2012.

[4] Boudaoud, A. Burian, D. Borowska-Wykręt, M. Uyttewaal, R. Wrzalik, D. Kwiatkowska and O. Hamant, "FibrilTool, an ImageJ plug-in to quantify fibrillar structures in raw microscopy images", Nature Protocols, vol. 9, no. 2, pp. 457-463, 2014.

[5] V. Piazza, B. Weinhausen, A. Diaz, C. Dammann, C. Maurer, M. Reynolds, M. Burghammer and S. Köster, "Revealing the Structure of Stereociliary Actin by X-ray Nanoimaging", ACS Nano, vol. 8, no. 12, pp. 12228-12237, 2014.

[6] Herman, "Extracellular matrix-cytoskeletal interactions in vascular cells", Tissue and Cell, vol. 19, no. 1, pp. 1-19, 1987.

[7] R. Ishikawa, T. Sakamoto, T. Ando, S. Higashi-Fujime and K. Kohama, "Polarized actin bundles formed by human fascin-1: their sliding and disassembly on myosin II and myosin V in vitro", Journal of Neurochemistry, vol. 87, no. 3, pp. 676-685, 2003.

[8] Vrabioiu and T. Mitchison, "Structural insights into yeast septin organization from polarized fluorescence microscopy", Nature, vol. 443, no. 7110, pp. 466-469, 2006.

[9] M. Müller, C. Czihak, G. Vogl, P. Fratzl, H. Schober and C. Riekel, "Direct Observation of Microfibril Arrangement in a Single Native Cellulose Fiber by Microbeam Small-Angle X-ray Scattering", Macromolecules, vol. 31, no. 12, pp. 3953-3957, 1998.

[10] M. Beil, H. Braxmeier, F. Fleischer, V. Schmidt and P. Walther, "Quantitative analysis of keratin filament networks in scanning electron microscopy images of cancer cells", Journal of Microscopy, ol. 220, no. 2, pp. 84-95, 2005.

[11] J. Weichsel, E. Urban, J. Small and U. Schwarz, "Reconstructing the orientation distribution of actin filaments in the lamellipodium of migrating keratocytes from electron microscopy tomography data", Cytometry Part A, vol. 81, no. 6, pp. 496-507, 2012.

[12] Rigort, D. Günther, R. Hegerl, D. Baum, B. Weber, S. Prohaska, O. Medalia, W. Baumeister and H. Hege, "Automated segmentation of electron tomograms for a quantitative description of actin filament networks", Journal of Structural Biology, vol. 177, no. 1, pp. 135-144, 2012.

[13] T. Xu, D. Vavylonis, F. Tsai, G. Koenderink, W. Nie, E. Yusuf, I-Ju Lee, J. Wu and X. Huang, "SOAX: A software for quantification of 3D biopolymer networks", Scientific Reports, vol. 5, p. 9081, 2015.